

Simulation research on surface growth process of positive and negative frequency detuning chromium atom lithographic gratings

Zhi-Jun Yin(尹志珺), Zhao-Hui Tang(唐朝辉), Wen Tan(谭文), Guang-Xu Xiao(肖光旭),Yu-Lin Yao(姚玉林), Dong-Bai Xue(薛栋柏), Zhen-Jie Gu(顾振杰), Li-Hua Lei(雷李华),Xiong Dun(顿雄), Xiao Deng(邓晓), Xin-Bin Cheng(程鑫彬), and Tong-Bao Li(李同保)

Citation: Chin. Phys. B, 2023, 32 (**10**): 100601. DOI: 10.1088/1674-1056/ace95b
Journal homepage: http://cpb.iphy.ac.cn; http://iopscience.iop.org/cpb

What follows is a list of articles you may be interested in

Feedback control and quantum error correction assisted quantum multi-parameter estimation

Hai-Yuan Hong(洪海源), Xiu-Juan Lu(鲁秀娟), and Sen Kuang(匡森)
Chin. Phys. B, 2023, 32 (**4**): 040603. DOI: 10.1088/1674-1056/ac8721

Effective sideband cooling in an ytterbium optical lattice clock

Jin-Qi Wang(王进起), Ang Zhang(张昂), Cong-Cong Tian(田聪聪), Ni Yin(殷妮), Qiang Zhu(朱强), Bing Wang(王兵), Zhuan-Xian Xiong(熊转贤), Ling-Xiang He(贺凌翔), and Bao-Long Lv(吕宝龙)
Chin. Phys. B, 2022, 31 (**9**): 090601. DOI: 10.1088/1674-1056/ac5392

Characterization of a nano line width reference material based on metrological scanning electron microscope

Fang Wang(王芳), Yushu Shi(施玉书), Wei Li(李伟), Xiao Deng(邓晓), Xinbin Cheng(程鑫彬), Shu Zhang(张树), and Xixi Yu(余茜茜)
Chin. Phys. B, 2022, 31 (**5**): 050601. DOI: 10.1088/1674-1056/ac3225

Optimization of laser focused atomic deposition by channeling

Jie Chen(陈杰), Jie Liu(刘杰), Li Zhu(朱立), Xiao Deng(邓晓), Xinbin Cheng(陈鑫彬), Tongbao Li(李同保)
Chin. Phys. B, 2020, 29 (**2**): 020601. DOI: 10.1088/1674-1056/ab631c

Fabrication and measurement of traceable pitch standard with a big area at trans-scale

Deng Xiao (邓晓), Li Tong-Bao (李同保), Lei Li-Hua (雷李华), Ma Yan (马艳), Ma Rui (马蕊), Weng Jun-Jing (翁浚婧), Li Yuan (李源)
Chin. Phys. B, 2014, 23 (**9**): 090601. DOI: 10.1088/1674-1056/23/9/090601

Simulation research on surface growth process of positive and negative frequency detuning chromium atom lithographic gratings

Zhi-Jun Yin(尹志珺)[1,2,3,4,5], Zhao-Hui Tang(唐朝辉)[1,2,3,4,5], Wen Tan(谭文)[1,2,3,4,5], Guang-Xu Xiao(肖光旭)[1,2,3,4,5], Yu-Lin Yao(姚玉林)[1,2,3,4,5], Dong-Bai Xue(薛栋柏)[1,2,3,4,5], Zhen-Jie Gu(顾振杰)[1,2,3,4,5], Li-Hua Lei(雷李华)[6], Xiong Dun(顿雄)[1,2,3,4,5], Xiao Deng(邓晓)[1,2,3,4,5,†], Xin-Bin Cheng(程鑫彬)[1,2,3,4,5], and Tong-Bao Li(李同保)[1,2,3,4,5]

[1] *Institute of Precision Optical Engineering, Tongji University, Shanghai* 200092, *China*
[2] *School of Physics Science and Engineering, Tongji University, Shanghai* 200092, *China*
[3] *MOE Key Laboratory of Advanced Micro-Structured Materials, Shanghai* 200092, *China*
[4] *Shanghai Frontiers Science Center of Digital Optics, Shanghai* 200092, *China*
[5] *Shanghai Professional Technical Service Platform for Full-Spectrum and High-Performance Optical Thin Film Devices and Applications, Shanghai* 200092, *China*
[6] *Shanghai Institute of Measurement and Testing Technology, Shanghai* 201203, *China*

(Received 7 March 2023; revised manuscript received 14 July 2023; accepted manuscript online 21 July 2023)

Chromium atom photolithography gratings are a promising technology for the development of nanoscale length standard substances due to their high accuracy, uniformity, and consistency. However, the inherent difference between the interaction of positive and negative frequency detuning standing wave field and the atoms can cause a difference in the adjacent peak-to-valley heights of the grating in positive and negative frequency detuning chromium atom lithography, which greatly reduces its accuracy. In this study, we performed a controlled variable growth simulation using the semi-classical theoretical model and Monte Carlo method with trajectory tracking and ballistic deposition methods to investigate the influence of key experimental parameters on the surface growth process of positive and negative frequency detuning atomic lithography gratings. We established a theoretical model based on simulation results and summarized empirical equations to guide the selection of experimental parameters. Our simulations achieved uniform positive and negative frequency detuning atomic lithography gratings with a period of 1/4 of the wavelength corresponding to the atomic transition frequency, and adjacent peak-to-valley heights differing by no more than 2 nm, providing an important theoretical reference for the controllable fabrication of these gratings.

Keywords: self-traceable grating, atom lithography, positive and negative frequency detuning, surface growth

PACS: 06.20.–f, 11.15.Kc, 42.79.Dj, 43.25.Gf **DOI:** 10.1088/1674-1056/ace95b

1. Introduction

At present, nanotechnology is gradually developing towards a smaller feature size, which makes it very urgent to solve the problem of precise measurement at the nanoscale, especially the precise calibration of nanoscale measuring instruments.[1] Therefore, the development of accurate and applicable nanometric transfer standards has become a key link in nanotechnology.[2] The traceability of nanoscale length values involves linking measurements to international or national metrology standards via a traceability chain, enabling accurate, reliable, and repeatable measurements.[3,4] In 1999, the Bureau International des Poids et Mesures (BIPM) designated the wavelength of light output by a frequency-stabilized laser as the international standard spectral line of meter in the Metre Convention, serving as a metrology reference for calibrating nano-meter measuring instrument. The traceability transmission chain of nanometer measurement directly traces the measurement result to the definition of meter, but it still needs the accurate nanoscale standard template. The photolithographic grating of chromium atoms deposited by the Gaussian standing wave optical field can be used as a self-traceable length standard substance, self-traceable from the energy level transition frequency of chromium atoms. With extremely high accuracy, uniformity and consistency, it directly calibrates daily measuring instruments and effectively shortens the traceability chain.[5–7] In particular, the 26th Conférence générale des poids et mesures (CGPM) in 2018 redefined the 7 basic units of Système International d'Unités (SI) based on constant natural constants.[8] This means that the atomic lithography technology, which is traced back to the basic natural constants, is of great significance to the development of metrology equipment detection.

The traditional one-dimensional atomic lithography technology can be utilized to prepare one-dimensional self-traceable gratings with a period of $\lambda/2$, whose period is self-traced to the wavelength corresponding to the transition energy level $^7S_3 \rightarrow {}^7P_4^0$ of the chromium atom[9,10], and has been recognized as a national first-class standard substance with a nanometer length.[11] In order to reduce the pitch further, three methods have been proposed: positive and negative frequency detuning,[12–14] polarization gradient,[15] and

†Corresponding author. E-mail: 18135@tongji.edu.cn
© 2023 Chinese Physical Society and IOP Publishing Ltd

multi-beam interference.[16] The latter is mainly utilized for the preparation of gratings with hexagonal lattice points. On the other hand, both positive and negative frequency detuning and polarization gradient methods can prepare atomic photolithography gratings with a period of $\lambda/4$. The positive and negative frequency detuning method uses the principle that the positive and negative frequency detuning standing wave fields can respectively gather atoms at the nodes and antinodes. Meanwhile, the latter needs to consider the alternating current (AC) Stark effect of atoms in the laser standing wave field, necessitating a small amount of laser detuning and strict polarization control.[17] Compared to the polarization gradient method, the positive and negative frequency detuning method is more experimentally feasible, easier to form a stable $\lambda/4$ period grating structure, and realize the spatial frequency doubling of the $\lambda/2$ period grating.

In the positive frequency detuning standing wave field, atoms experience stronger convergence and are deposited at the nodes of the optical field. Conversely, in the negative frequency detuning standing wave field, atoms experience weaker convergence and are deposited at the antinodes. As a result, differences in the convergence ability of positive and negative frequency detuning standing wave fields on atoms can lead to variations in the height and full width at half maximum (FWHM) of adjacent grid lines of the atomic lithography grating. One-dimensional chromium atom photolithographic gratings used as nanoscale length standard substances require extremely high uniformity, since non-uniform gratings can significantly impact the precise calibration of metrological measuring instruments. For instance, uneven heights of grating lines can cause a wave phase difference in diffracted light, leading to a decrease in the measurement accuracy of the grating interferometer. Additionally, chromium atom lithography grating can also serve as a mask for soft x-ray interference lithography to fabricate large-area nanoscale periodic structures such as lines, holes, and columns. However, the uneven height of the grating lines will reduce the diffraction efficiency of the grating and affect the quality of the sample.

To reduce feature differences between adjacent grid lines of the photolithography grating, the deposition characteristics of positive and negative frequency detuning chromium atom photolithographic gratings were investigated in depth, and the growth process of gratings was simulated with control variables. Based on the simulation results, the effects of controllable laser parameters such as laser power, Gaussian beam waist radius, and detuning, on the focal point of atomic lithography deposition were quantitatively analyzed. An empirical equation was derived from the focallocating method to summarize the dependence of laser parameters on the focal point position. Consequently, a method for achieving uniformity of positive and negative frequency detuning atomic lithographic gratings was developed, which provides a theoretical reference for the development of high uniformity positive and negative frequency detuning atomic lithographic gratings.

2. Theory

2.1. Semi-classical theory

Atomic lithography is based on the interaction between atoms and light, which can occur through two mechanisms: spontaneous force and dipole force.[18] Spontaneous force is generated by the recoil momentum resulting from the emission of a photon when an excited atom transitions to a lower energy state. This principle is used to achieve Doppler cooling of atoms in atomic lithography experiments, which is commonly employed to reduce the lateral velocity of atoms and achieve collimated atomic beams.[19,20] Dipole force is critical to atomic lithography. When an atom is exposed to an optical field with varying spatial electric field strength, it experiences a dipole force proportional to the gradient of the electric field strength, represented as $F = -\nabla U$. Therefore, dipole forces arise when the light intensity distribution is not uniform. The typical case is Gaussian laser optical fields, which are also simulated in this paper.

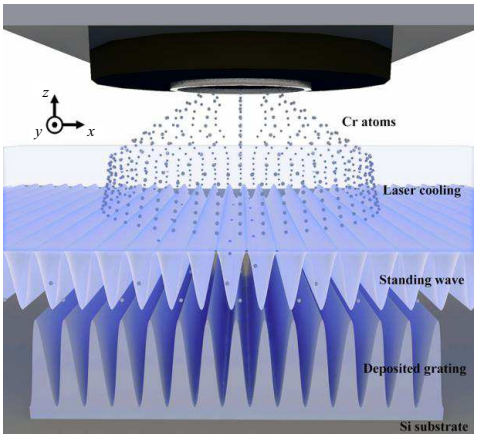


Fig. 1. Schematic of atomic lithography. Atoms are ejected in the z-direction and then collimated by laser cooling. Affected by the convergence of the laser standing wave field distributed in the x direction, the grating is deposited on the substrate.

To describe atomic motion in a natural environment, it is necessary to analyze it from a quantum perspective and build a model under the semi-classical theory.[21] When the laser light intensity is small and detuning is large, the probability of atomic transition to the excited state and the spontaneous emission rate are small. Therefore, the influence of the excited state atom can be ignored, and the dipole force is dominant in the interaction between atoms and light. The two-level atom can be considered to move in a conservative potential field, and the potential energy of the ground state atom can be expressed as[22,23]

$$U(x,y,z) = \frac{\hbar\gamma^2}{8\Delta}\frac{I(x,y,z)}{I_s}, \tag{1}$$

where $\hbar = h/2\pi$ is the reduced Planck constant, γ is the natural linewidth of the atomic transition, Δ is the detuning of the laser frequency from the atomic transition frequency, I_s is the saturation intensity associated with the atomic transition. $I(x,y,z)$ is the laser intensity.

From Eq. (1), it can be intuitively explained why atoms deposit at the nodes and antinodes in positive and negative frequency detuning optical fields, respectively. When $\Delta > 0$, the potential energy is the smallest at the minimum optical field intensity, and atoms move to the minimum light intensity and deposit at nodes. Conversely, the potential energy is the smallest whereas the light intensity is the largest, so atoms are deposited at the antinodes when $\Delta < 0$. Under the effect of positive and negative detuning optical fields, atoms depositing at nodes and antinodes respectively form two gratings with a pitch of $\lambda/2$, which can effectively double the spatial frequency of the current one-dimensional self-traceable grating with a pitch of $\lambda/2$.

A deeper optical potential well allows atoms to exhibit better periodic arrangements. It can be seen from Eq. (1) that the potential well depth can be effectively increased by increasing the light intensity and reducing the detuning. However, when the detuning amount is too small, the influence of spontaneous emission cannot be ignored. Therefore, two conditions need to be guaranteed.

(i) The movement speed of atoms in the spatially varying laser field is sufficiently slow to maintain adiabaticity at all times.

(ii) The time that atoms remain in the optical field is insufficient to induce spontaneous radiation that would significantly alter their trajectory

$$(v_z/I)(\mathrm{d}I/\mathrm{d}z) \ll \gamma, \quad (l/v_z) \gg \gamma^{-1}, \tag{2}$$

where $1/\gamma$ is the time scale for spontaneous radiation of atoms returning to equilibrium, v_z is the characteristic velocity of atoms in the z-axis direction, l is the characteristic length at which atoms interact with the optical field. After approximate simplification, the atomic potential energy can be expressed as

$$U(x,y,z) = \frac{\hbar\Delta}{2}\ln[1+p(x,y,z)], \tag{3}$$

where

$$p(x,y,z) = \frac{I(x,y,z)}{I_s}\frac{\gamma^2}{\gamma^2+4\Delta^2} = p_0 G(x,y,z),$$

$$G(x,y,z) = g(y,z)\sin^2 kx = \exp\left(-\frac{2(z^2+y^2)}{w(x)^2}\right)\sin^2 kx,$$

which is a dimensionless function of the spatial components in $p(x,y,z)$, $k = 2\pi/\lambda$ is the light wave vector, $w(x) = w_0\sqrt{1+(x/x_R)^2}$ is the space-varying beam width of the Gaussian light, w_0 is the beam waist, x_R is the Rayleigh length, $p_0 = (I_0/I_s)(\gamma^2/(\gamma^2+4\Delta^2))$ is the light parameter component, and I_0 is the laser intensity at $G(x,y,z) = 1$.

2.2. Principle of trajectory tracking

Considering the atomic motion in a laser standing wave, we first assume that the model along the y direction has translational symmetry, and any optical force along this direction can be neglected compared to the dipole force produced by the laser standing wave on the atom. Therefore, we simplify the atom deposition model to a two-dimensional motion problem in the x and z directions, and can derive the Lagrange equation of the atom in the laser standing wave

$$L = \frac{1}{2}m(\dot{x}+\dot{z})^2 - U(x,z), \tag{4}$$

where m is the mass of the chromium atom, $\dot{x}$ and $\dot{z}$ are the velocities of the atom in the x and z directions, respectively. Throughout the process, the motion of the atom in the laser standing wave is a conservative system, and the total energy of the atom remains unchanged. Then, using the Lagrange equation of the conservative system

$$\begin{cases} \dfrac{\mathrm{d}}{\mathrm{d}t}\left(\dfrac{\partial L}{\partial \dot{x}}\right) - \dfrac{\partial L}{\partial x} = 0, \\ \dfrac{\mathrm{d}}{\mathrm{d}t}\left(\dfrac{\partial L}{\partial \dot{z}}\right) - \dfrac{\partial L}{\partial z} = 0, \end{cases} \tag{5}$$

the equation of motion of the atom in the standing wave can be simplified as

$$\begin{cases} \ddot{x} + \dfrac{1}{m}\dfrac{\partial U(x,z)}{\partial x} = 0, \\ \ddot{z} + \dfrac{1}{m}\dfrac{\partial U(x,z)}{\partial z} = 0. \end{cases} \tag{6}$$

After eliminating the time component, a function of x and z can be obtained as

$$x'' = \frac{1+x'^2}{2(E_0-U)}\left(x'\frac{\partial U}{\partial z} - \frac{\partial U}{\partial x}\right), \tag{7}$$

where $x' = \mathrm{d}x/\mathrm{d}z$, $x'' = \mathrm{d}x'/\mathrm{d}z$, and E_0 is the total energy of the atom. To simulate atom's motion trajectory in the laser standing wave, Eq. (3) is substituted into Eq. (7), and numerical methods are used for calculation. The simulation utilizes the fourth-order Runge–Kutta methods (RK4) to solve the atom's motion trajectory.

In order to make the model better simulate the trajectory of atoms in the real situation, this study uses the Monte Carlo method to set the initial state of the atoms. First, obtain a set of random numbers (x_i, v_i, α_i) to set the ejection conditions of the atoms, where x_i is the initial position of the atoms ejected, by selecting a random number in the range of $[-0.25n\lambda, 0.25n\lambda]$, and n represents the number of periods selected. v_i is the initial longitudinal velocity of the atoms, used to set the initial kinetic energy. α_i is the atom initial divergence angle. After selecting

the atomic emission conditions, use the following equation to determine the flux probability of atoms:

$$P(v_{\rm i},\alpha_{\rm i}) \propto v_{\rm i}^4 \exp\left[-\frac{v_{\rm i}^2}{2v_0^2}\left(1+\frac{\alpha^2}{2\alpha_0^2}\right)\right], \tag{8}$$

where v_0 is the most probable longitudinal velocity of atoms, $\alpha_{\rm FWHM}$ is the half-peak width of the divergence angle distribution of the atomic beam in the laser cooling experiment $\alpha_0 = \alpha_{\rm FWHM}/(2\sqrt{\sqrt{2}-1})$. Substitute the obtained random number $(x_{\rm i}, v_{\rm i}, \alpha_{\rm i})$ into the calculation formula of flux probability to get $P(v_{\rm i},\alpha_{\rm i})$. Select a random number $P_{\rm i}$ in the range of $[0, P(v_0,\alpha_0)]$, and if $P_{\rm i} < P(v_{\rm i},\alpha_{\rm i})$, it is considered that the atomic emission condition is met, and the trajectory of the atom in the standing wave field is calculated. Otherwise, a random number is selected again.

In addition, this paper also considers the influence of various natural isotopes of chromium on the calculation of grating deposition structure. Among the various natural isotopes of chromium, the abundance of atoms ^{52}Cr is about 84%, while the sum of other isotopes only accounts for 16% and they will not interact with the laser standing wave field. To consider the effect of other isotopes on grating structure, we choose a random number between 0 and 1, if it is less than 0.16, the atom is considered to be an isotope of ^{52}Cr.

In calculating the growth process of the atomic lithography grating surface topography, we use the ballistic deposition (BD) method in the molecular beam epitaxy model to obtain the atomic deposition position closer to the actual situation, as shown in Fig. 2.

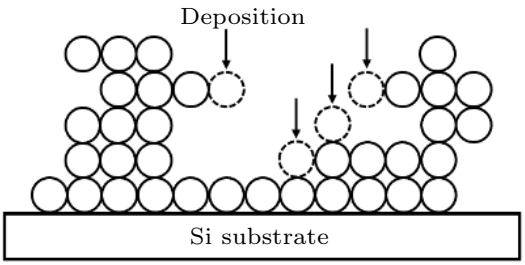


Fig. 2. Schematic of ballistic deposition method.

The most notable feature of the BD model is that atoms stick together as long as they are nearby during deposition.[24] To accurately describe the arrangement of chromium atoms in space, we use the unit cell size of chromium atoms to represent the smallest repeating structure that is regularly arranged in the crystal. Chromium has a body-centered cubic structure, and its lattice constant is denoted as $L = 0.2884$ nm, and the number of atoms $N \approx 738$ can be arranged in a single layer within the half-wavelength range. As atom deposition is a continuous process and the trajectory is not perpendicular to the substrate, we optimize the BD model by using a step-by-step positioning method to gradually decompose the motion path of the atom at each calculation step according to the rule of first horizontal and then vertical. This creates a continuous motion trajectory. By determining the deposition position of each atom, we can obtain the surface topography image of the chromium atom photolithographic grating. In addition, considering the high stability of chromium atoms, the effects of factors such as mesa diffusion and edge sinking of atoms are omitted in the numerical simulation. Figure 3 shows the complete process steps of the above surface growth calculation.

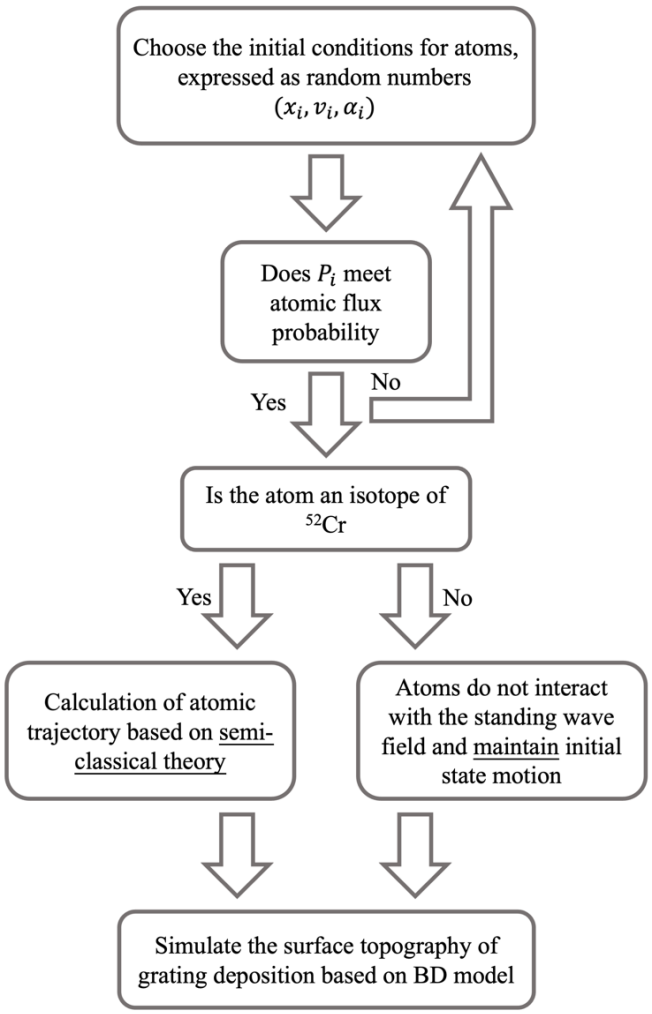


Fig. 3. Flow chart of trajectory tracking method simulation program.

As shown in Fig. 4, the movement trajectory of 50 chromium atoms under the action of dipole force inside the laser standing wave field is presented. The focal point of the atomic beam is formed by the convergence of the laser standing wave field, similar to an optical lens. The characteristic size of the grating is directly related to the ability of the light field to converge on the atoms. Therefore, we believe that the deposition position should be selected near the focal point to obtain grating lines with higher height and narrower half-maximum width. In the next section, we analyze the multiple factors that affect convergence and look for ways to achieve positive and negative frequency detuning grating uniformity.

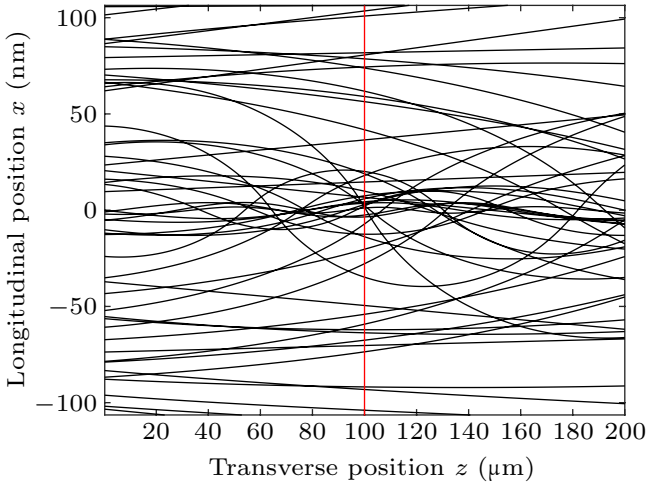


Fig. 4. The trajectory of atoms in the range of laser standing wave field. Under the convergence of the light field, trajectories of atoms form a focal position near the red line $f = 100$ μm. Simulation parameters are $\lambda = 425.55$ nm, $P = 50$ mW, $w_0 = 100$ μm, $\Delta = +250$ MHz, $I_s = 85$ W/m^2, $\gamma = 3.15 \times 10^7$ rad/s.

3. Simulation results

Based on the semiclassical theoretical model, the deposition of atoms under positive and negative frequency detuning optical fields occurs at node and antinode positions, respectively, due to the different interactions with the standing wave field. It is reflected as the difference in the converging ability of the positive and negative frequency detuning light fields, resulting in inconsistency in adjacent grating heights. The concentration ability of the standing wave field on atoms can be quantitatively analyzed by determining the focal point of the atomic beam under the influence of the standing wave field. Therefore, this section analyzes the converging ability of the light field from the perspective of experimental controllable factors, locates the focal point, and examines the effective methods for obtaining a high-uniformity atomic lithography grating using positive and negative detuning.

In the semiclassical model, the grating line profile mainly depends on the laser power, Gaussian beam waist radius and detuning. In addition, slight differences in laser wavelength between the positive and negative detuning deposition experiments can also cause non-uniformity in grating pitch. The atomic flux is also an important factor affecting the change of the grating structure, including blockage of the atomic furnace tube, agglomeration of the chromium atoms, and interaction between chromium atoms during the atomic beam injection. This chapter mainly analyzes the reasons that affect the uniformity of chromium atom photolithography grating from the perspective of laser parameters. In the numerical simulation, only the deposition trajectory simulation of the single atom is considered, and the interaction of atoms in the deposition process is ignored, while it should be taken into account when the flux is high.

3.1. Effect of laser power on growth

Laser power P is a crucial experimental parameter. As shown in Fig. 5(a), the potential energy distribution of chromium atoms in the standing wave field changes with laser power. When laser power is small, the potential energy gradient of the atoms in the positive and negative frequency detuning standing wave fields is basically the same. However, as the laser power increases, the potential energy gradient of atoms at the nodes of the positive detuning field becomes larger. By fitting the potential energies of the atom deposition positions in the positive and negative detuning fields respectively, the magnitudes of the potential energy gradients of the two can be compared. At the node, there is $kx \ll 1$, the atomic potential energy simplifies to

$$U_{\text{node}} = \frac{\hbar\Delta}{2} p_0 g(y,z)(kx)^2. \tag{9}$$

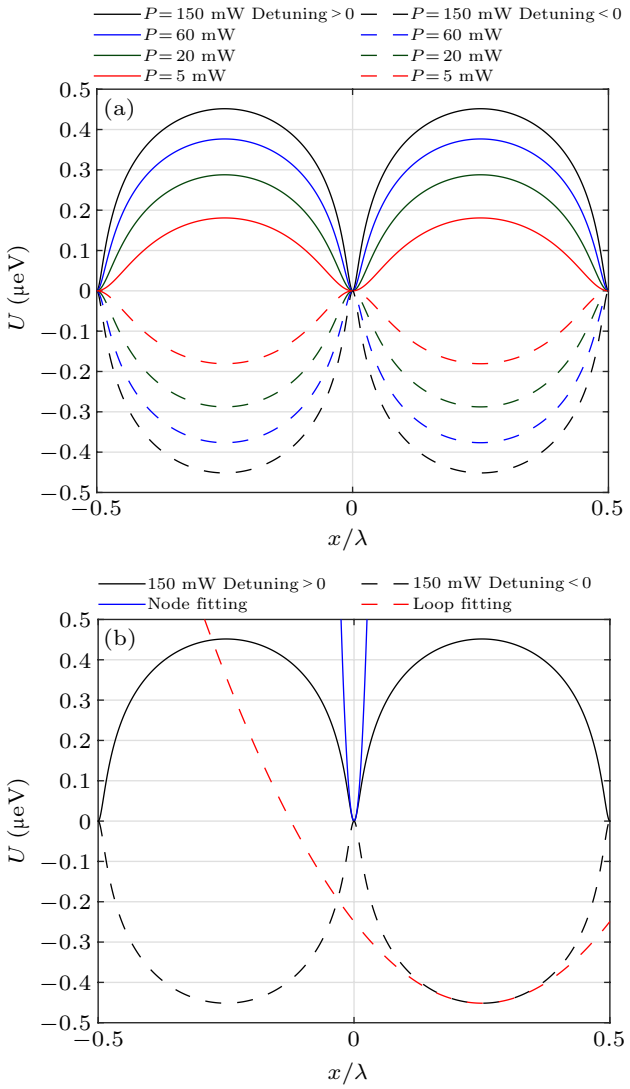


Fig. 5. The effect of laser power on atomic potential energy. (a) The potential energy of positive and negative frequency detuning atoms at different laser powers. (b) Comparison of fitting of atomic potential energy at nodes of positive detuning and antinodes of negative detuning when laser power is $P = 150$ mW. The gradient of fitting curves reflects the convergence ability of the light field on atoms.

The atomic potential energy near the antinode in the negative detuned field is expressed as

$$U_{\text{loop}} = \frac{\hbar\Delta}{2}\left[\frac{p_0 g(y,z)(kx)^2}{1+p_0 g(y,z)} - \ln(1+p_0 g(y,z))\right]. \quad (10)$$

In Fig. 5(b), the blue solid line is the potential energy fitting line of atoms at the node of the positive detuning field, and the red dashed line is the potential energy fitting line of atoms at the antinode of the negative detuning field. It can be concluded that when $P = 150$ mW, atoms experience greater converging action at the node of the positive detuning optical field and less converging action at the antinode of the negative detuning optical field.

Differences in the ability of light fields to converge atoms can cause differences in the feature sizes of adjacent gratings. It can be seen from Fig. 5(a) that under the conditions of $\Delta = \pm 250$ MHz and $w_0 = 100$ μm, as laser power increases, the atomic potential energy gradient will increase, and the difference between positive and negative detuned optical fields on the convergence ability of atoms will be more obvious. Even at lower laser powers, the difference in converging power is reduced but cannot be completely eliminated.

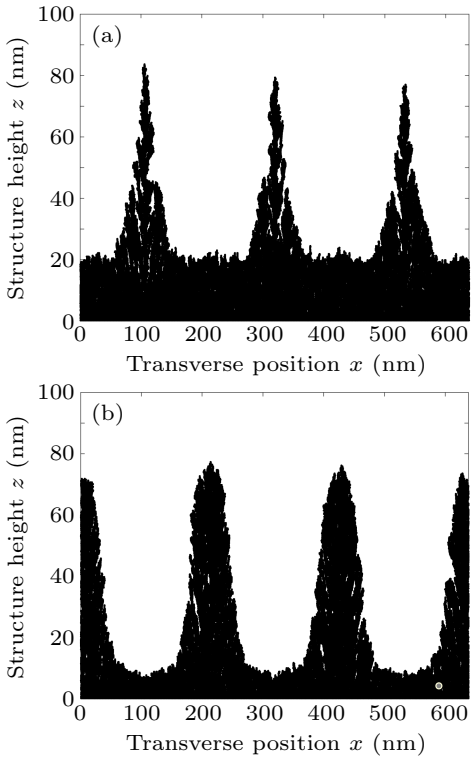


Fig. 6. Surface morphology comparison of positive and negative frequency detuning gratings in the three half-wavelength ranges. The parameters $P = 150$ mW, $\Delta = \pm 250$ MHz, and $w_0 = 100$ μm. (a) Surface morphology of positively frequency detuning grating. (b) Surface morphology of the negatively frequency detuning grating.

Figure 6 shows a simulation of the surface morphology of grating lines within the range of three standing wave periods under positive and negative frequency detuning light fields. The total number of deposited atoms is 110850, and the deposition positions are all located near the focus position f. The positive detuning deposition position is $f_x = 150$ μm, and the negative detuning deposition position is $f_x = 210$ μm, which means compared with the negative detuned optical field, the positive detuned optical field has a stronger ability to converge atoms, which is consistent with the theoretical speculation. Among them, $f_x = 0$ means that the deposition position is just at the edge of the laser beam waist radius close to the atomic beam. The average FWHM of positively frequency detuning grating lines is 37 nm, and the average height is 56 nm, while the average FWHM of negatively frequency detuning grating lines is 72 nm, and the average height is 65 nm. From the simulation results, it can be seen that at higher laser power, the difference in the convergence ability of positive and negative frequency detuning optical fields to atoms causes noticeable differences in the structure of the grating lines, particularly in the height difference.

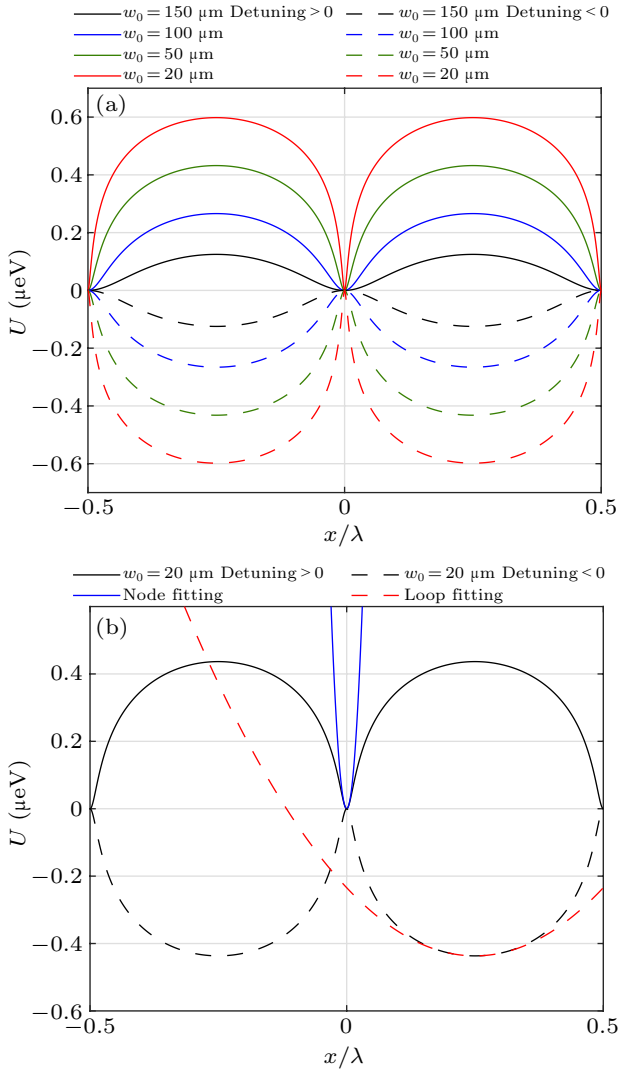


Fig. 7. The effect of Gaussian beam waist radius on atomic potential energy. (a) Potential energy of positive and negative frequency detuning atoms at different beam waist radius. (b) Comparison of fitting of atomic potential energy at nodes of positive detuning and antinodes of negative detuning when the beam waist radius is $w_0 = 20$ μm.

3.2. Effect of waist radius of Gaussian beam on growth

The effect of the Gaussian beam waist radius w_0 on the atomic potential energy is shown in Fig. 7(a). As the beam waist radius increases, the potential energy gradient decreases gradually at the nodes of the positive detuning optical field and the antinodes of the negative detuning optical field. When the beam waist radius is small, there is a significant difference in the potential energy gradient between the two, leading to the formation of an inhomogeneous positive and negative detuning grating. Figure 7(b) compares the atomic potential energy gradient at the nodes of positive detuning and antinodes of negative detuning. When the beam waist radius is large, although the atomic potential energy gradient is similar, the convergence ability of the light field is weak, resulting in a low utilization rate of atoms and affecting the height of the grating.

Figure 8 shows the results of a deposition simulation experiment using 110850 atoms. The simulation sets $P = 50$ mW to reduce the difference in the convergence ability of the light field caused by high power. The positive detuning deposition position is $f_x = 40$ μm, and the negative detuning deposition position is $f_x = 200$ μm. The simulation results show that the FWHM of positively detuning grating lines is 26 nm, with an average height is 39 nm. The average FWHM of negatively detuning grating lines is 100 nm, with an average height is 49 nm.

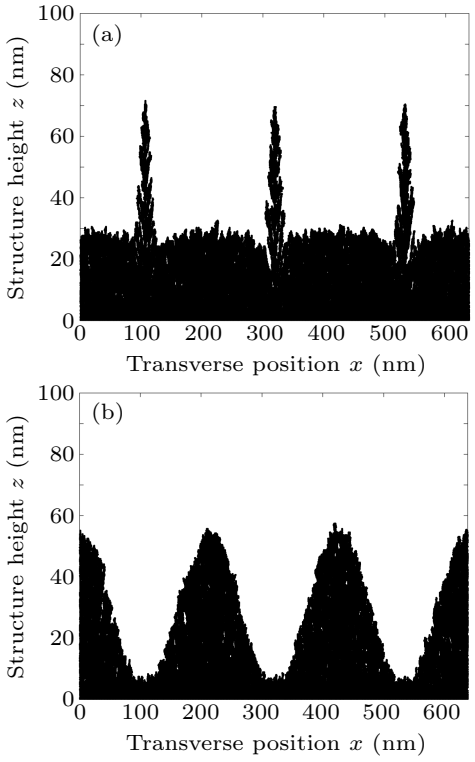


Fig. 8. Surface morphology comparison of positive and negative frequency detuning gratings in the three half-wavelength ranges. The parameters $P = 50$ mW, $\Delta = \pm 250$ MHz, and $w_0 = 20$ μm. (a) Surface morphology of positive frequency detuning grating. (b) Surface morphology of negative frequency detuning grating.

While it is possible that the small size and weak convergence of atoms receiving the light field contributed to these results, it can still be inferred that a smaller beam waist radius leads to a significant difference in the convergence ability of positive and negative detuning optical fields to atoms. Additionally, the reduction of the laser beam waist radius can effectively reduce the FWHM of the grid lines under positive detuning conditions, as demonstrated in the power group comparison. On the other hand, compared with the simulation experiment of the power group, the change of beam waist radius also causes the change of focus point position f. The essence is that the compound parameter, power density, formed by the laser power and the beam waist radius affect the convergence effect of the light field on the atoms. However, in the experiment, it is difficult to accurately grasp the change of power density, but the change of power density can be indirectly controlled by modifying the laser power and the size of the beam waist radius, which will be explained in the fourth section.

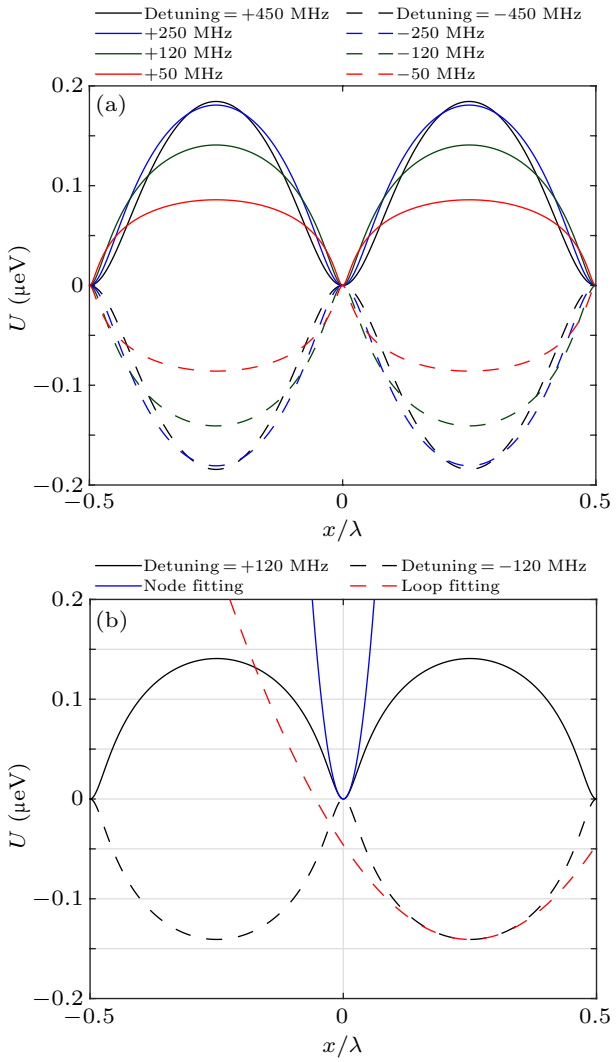


Fig. 9. The effect of detuning on atomic potential energy. (a) Potential energy of positive and negative frequency detuning atoms at different detuning. (b) Comparison of fitting of atomic potential energy at nodes of the positive detuning and antinodes of the negative detuning when detuning is $\Delta = \pm 120$ MHz.

3.3. Effect of optical field detuning on growth

Figure 9(a) shows the effect of laser detuning Δ on atomic potential energy. Unlike the previous parameters, the potential energy gradient at the nodes of the positively detuned optical field decreases with increasing detuning, while the potential energy gradient of the negatively detuned optical field increases with increasing detuning. Therefore, the reduction of the detuning amount can increase the difference in the convergence ability of the positive and negative detuning method, leading to higher inhomogeneity in photolithographic gratings formed by this method. Additionally, excessively high detuning can weaken the interaction between atoms and the light field, making it important to use an appropriate detuning amount to fabricate photolithographic gratings with high uniformity.

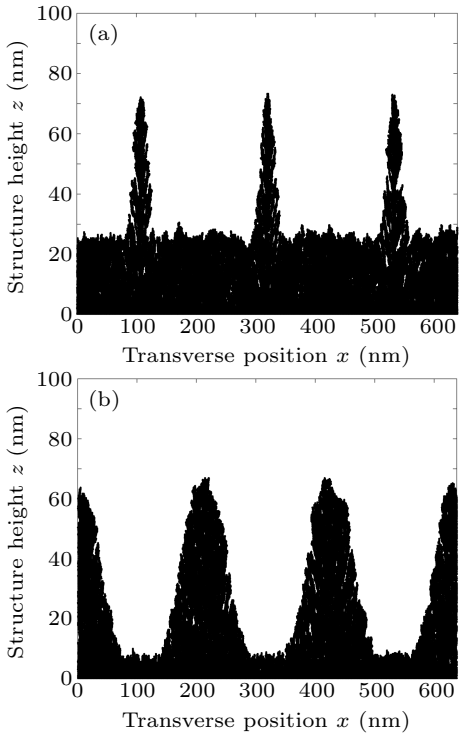


Fig. 10. Surface morphology comparison of positive and negative frequency detuning gratings in the three half-wavelength ranges. The parameters $P = 50$ mW, $\Delta = \pm 120$ MHz, and $w_0 = 100$ μm. (a) Surface morphology of positive frequency detuning grating. (b) Surface morphology of negative frequency detuning grating.

Simulation experiments were performed to compare the converging ability of positive and negative detuning light fields. Figure 10(b) shows the potential energy gradient difference at the positive detuning node and the negative detuning antinode when the detuning amount is $\Delta = \pm 120$ MHz, and Fig. 11 displays the simulated grating line structure under this parameter. The number of deposited atoms is 110850, with the positive detuning deposition position at $f_x = 100$ μm and the negative detuning deposition position at $f_x = 250$ μm. The average FWHM of the positively detuning grating lines is 32 nm, and the average height is 44 nm, while the average FWHM of the negatively detuning grating lines is 88 nm, with an average height of 57 nm. Combining the simulation results with the atomic potential energy distribution diagram, it can be concluded that when the amount of detuning is small, there is a significant difference in the converging ability of positive and negative detuned optical fields on atoms. As a result, this difference in converging ability leads to variations in the focus positions f and subsequently affects the formation of grating line structures.

3.4. Focallocating method

The simulation structure in the previous sections demonstrated that three physical quantities, laser power P, Gaussian beam waist radius w_0, and detuning Δ, affect the ability of the light field to converge atoms. It has been proved in the simulation experiment that the converging ability of the light field is intuitively manifested as the converging point formed by the trajectory of the atoms — the focus position f. In particular, laser-related parameters are actively controllable variables in experiments. Therefore, analyzing the influence of these three parameters on the focus position in detail is the best way to realize the control of the grating shape. At the same time, the appropriate experimental parameters can be effectively determined. This analysis can also be used to fabricate positive and negative detuning atomic lithography gratings to achieve higher uniformity.

Establish a theoretical relationship model between the focus position and laser parameters

$$f = f(P, w_0, \Delta). \tag{11}$$

In Fig. 11, the dependence of the focus position on the laser power P, the Gaussian beam waist radius w_0 and the detuning Δ are respectively simulated, where $f = w_0$ indicates that the focus position is exactly at the center of the laser spot. The atomic distribution density in the z direction is calculated to determine the focus position. When the channeling effect occurs, the first converging position generated after the ejection of chromium atoms is selected as the focus position.

The simulation calculation results show that under the condition of positive detuning, the focal point moves forward continuously with an increase in power, a decrease in beam waist radius, and a decrease in detuning. Under the condition of negative detuning, the focus moves forward continuously as the power increases, the beam waist radius decreases, and the detuning increases. Due to the inherent difference in convergence ability of positive and negative detuning light fields, the focus position of the atomic beam is mostly located at the center of the laser spot under positive detuned light fields, whereas it is located at the edge of the laser spot under negative detuning. In the experiment, the best deposition effect can be achieved by adjusting the relative position of the laser spot

and the deposition substrate, that is, the adjustment of the deposition position f_x is just near the focus position f.

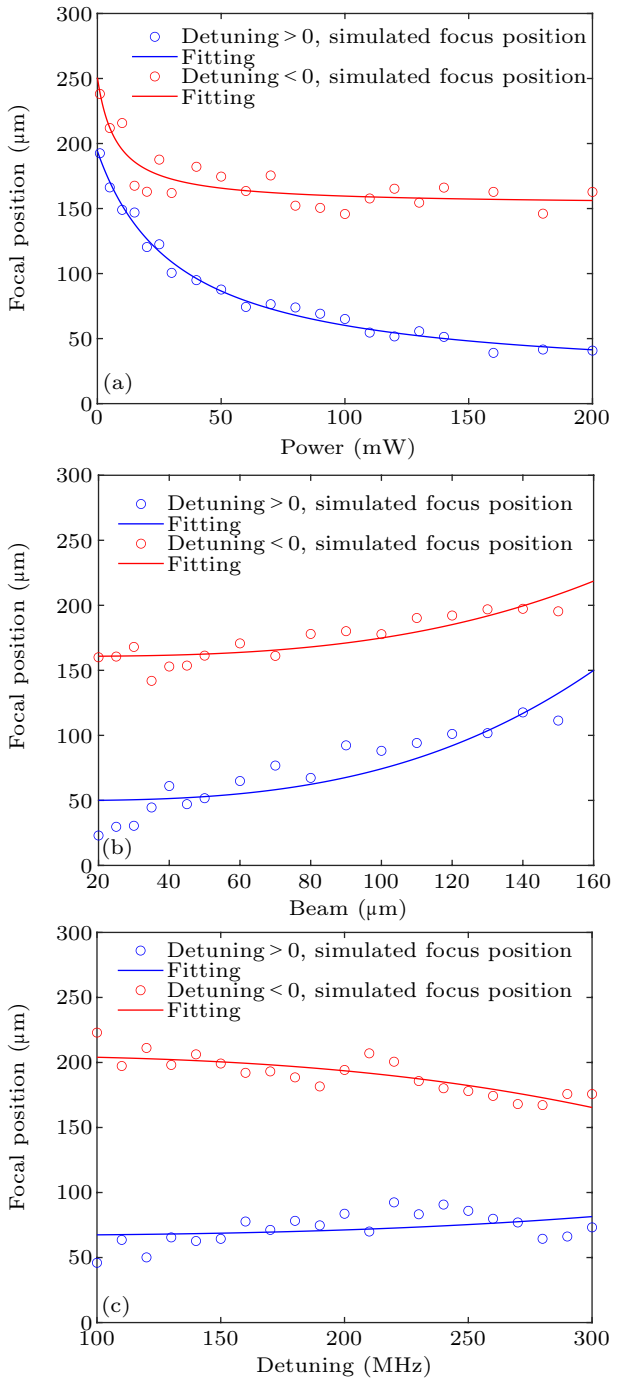


Fig. 11. Effect of laser parameters on focus position. Where the blue icon represents positive detuning data, and the red icon represents negative detuning data. The circles represent the simulated focal positions, and the solid lines represent the corresponding fitting curves. (a) Effect of laser power on the focus position, fixed parameter $w_0 = 100$ μm, $\Delta = \pm 250$ MHz. (b) Effect of beam waist radius on focus position, fixed parameters $P = 50$ mW, $\Delta = \pm 250$ MHz. (c) Effect of detuning amount on focus position, fixed parameters $P = 50$ mW, $w_0 = 100$ μm.

The empirical equation of focus position and laser parameters is obtained by fitting, which can provide a numerical reference for selecting relevant parameters in the experiment

$$f \propto [(P+a)^{-1}+b](w_0^3+c)(\Delta^3+d). \tag{12}$$

Among them, under positive detuning, the coefficients are $a = 32.57$, $b = 2.86 \times 10^{-3}$, $c = 2.04 \times 10^6$, $d = 1.24 \times 10^8$; under negative detuning, the coefficients are $a = 7.735$, $b = 0.201$, $c = 1.14 \times 10^6$, $d = -1.38 \times 10^8$. The calculation units of the laser parameters are mW, μm, and MHz, respectively. Based on this empirical equation, the approximate location of the focus under selected experimental parameters can be relatively determined. When the channeling effect occurs, the deposition location f_x can be selected after the focal location f, but is always within the range of the laser spot. In addition, the empirical equation provides the relative position of the focal point under a certain experimental setting, and the constant term should be analyzed and calculated according to the long-term experimental conclusion.

Based on the above conclusions, the high uniformity of positive and negative frequency detuning gratings can be achieved by selecting appropriate laser parameters and deposition location, and the effective frequency doubling grating spatial frequency can reach 106 nm. The simulation results are shown in Fig. 12.

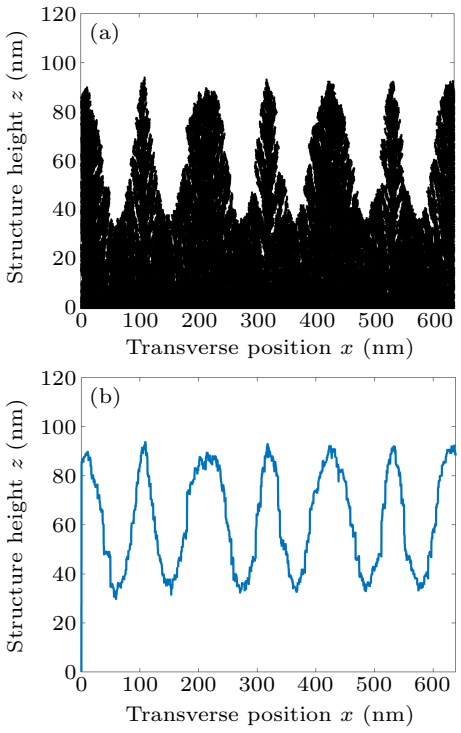


Fig. 12. The simulation diagram of atomic deposition of positive and negative detuning chromium atom photolithographic gratings. (a) Surface morphology of chromium atom photolithography grating. (b) Surface structure image of chromium atom photolithography grating.

For positive detuning, the deposition simulation is performed under $P = 50$ mW, $w_0 = 100$ μm, $\Delta = +250$ MHz, $f_x = 150$ μm, and for negative detuning, deposition simulation is carried out under the condition of $P = 150$ mW, $w_0 = 100$ μm, $\Delta = -250$ MHz, $f_x = 210$ μm. The deposition time ratio of positive and negative detuning is 3:2, and the total number of deposited atoms is 221700. The average FWHM

of the positively detuning grating is 39 nm, and the average feature height is 60 nm, whereas the average FWHM of the negatively detuning grating is 71 nm, and the average feature height is 58 nm. The key parameters of application research on gratings mainly include period and peak-to-valley height. However, because of the small pitch of positive and negative detuning atomic lithography gratings the application value of the grating is mainly focused on one-dimensional length calibration and precision equipment calibration. At present, the gravity center (GC) method[25] is the main method to accurately evaluate the pitch of one-dimensional gratings, and its calculation method mainly depends on the relative position of the top lines and bottom lines of the grating structure. The difference of FWHM contributes little to the pitch calculation, so the positive and negative disharmonic grating can still play its role in the actual instrument calibration.

4. Conclusion

The chromium atom photolithography grating plays an important role in the measurement and calibration of nanotechnology as a self-traceable length standard substance. The positive and negative frequency detuning chromium atom photolithography grating effectively doubles the spatial frequency of the grating, further improving the accuracy of measurement and calibration at the nanometer level. Based on trajectory tracking, the Monte Carlo method and BD model, this paper quantitatively analyzes the influence of key factors, such as laser power, Gaussian beam waist radius and detuning on positive and negative frequency detuning atomic lithography gratings, and forms an empirical equation to guide the selection of experimental parameters. In the final simulated deposition experiment of positive and negative frequency detuning gratings, the average FWHM of positive detuning grating lines is 39 nm, and the characteristic height is 60 nm; the average FWHM of negative detuning grating lines is 71 nm, and the characteristic height is 58 nm. Basically realizes the high uniformity of positive and negative frequency detuning chromium atom photolithography grating.

Acknowledgments

Project supported by the National Natural Science Foundation of China (Grant No. 62075165), the National Key Research and Development Program of China (Grant Nos. 2022YFF0607600 and 2022YFF0605502), the Special Development Funds for Major Projects of Shanghai Zhangjiang National Independent Innovation Demonstration Zone (Grant No. ZJ2021ZD008), the Shanghai Natural Science Foundation (Grant No. 21ZR1483100), the Shanghai Academic/Technology Research Leader (Grant No. 21XD1425000), and the Opening Fund of Shanghai Key Laboratory of Online Detection and Control Technology (Grant No. ZX2020101).

References

[1] Orji N G, Badaroglu M, Barnes B M, Beitia C, Bunday B D, Celano U, Kline R J, Neisser M, Obeng Y and Vladar A E 2018 *Nat. Electron.* **1** 532
[2] Dai G, Koenders L, Fluegge J and Bosse H 2016 *Opt. Eng.* **55** 091407
[3] Li T B 2005 *Shanghai Mea. & Test.* **185** 8 (in Chinese)
[4] Balykin V I and Letokhov V S 1987 *Opt. Commun.* **64** 151
[5] Deng X, Lin Z C, Dai G L, Tang Z H, Xie Z N, Xiao G X, Yin Z J, Lei L H, Jin T, Xue D B, Gu Z J, Cheng X B and Li T B 2023 arXiv: 2302.14633
[6] Deng X, Dai G, Liu J, Hu X, Bergmann D, Zhao J, Tai R, Cai X, Li Y, Li T and Cheng X 2021 *Ultramicroscopy* **226** 113293
[7] Liu J, Zhao J, Deng X, Yang S, Xue C, Wu Y, Tai R, Hu X, Dai G, Li T and Cheng X 2021 *Nanotechnology* **32** 175301
[8] Martin-Delgado M A 2020 *Eur. J. Phys.* **41** 063003
[9] Deng X, Li T B, Lei L H, Ma Y, Ma R, Weng J J and Li Y 2014 *Chin. Phys. B* **23** 090601
[10] Lei L, Li Y, Deng X, Fan G, Cai X, Cheng X, Weng J, Liu G and Li T 2015 *Sensor. Actuat. A-Phys.* **222** 184
[11] Deng X, Tan W, Tang Z, Lin Z, Cheng X and Li T 2022 *Nanomanuf. Metrol.* **5** 179
[12] Oberthaler M K and Pfau T 2003 *J. Phys.: Condens. Mat.* **15** R233
[13] McClelland J J and Celotta R J 2000 *Thin Solid Films* **367** 25
[14] Zhu L, Deng X, Liu J, Cheng X and Li T 2019 *Curr. Nanosci.* **15** 626
[15] Brezger B, Schulze T, Schmidt P O, Pfau R M T and Mlynek J 1999 *Europhys. Lett.* **46** 148
[16] Mützel M, Haubrich D and Meschede D 2000 *Appl. Phys. B* **70** 689
[17] Wang X, Deng X, Cai Y and Yang F 2020 *International Conference on Optoelectronic and Microelectronic Technology and Application* (China: Nanjing) p. 130
[18] McClelland J J, Scholten R E, Palm E C and Celotta R J 1993 *Science* **262** 877
[19] Dalibard J and Cohen-Tannoudji C 1989 *J. Opt. Soc. Am. B* **6** 2023
[20] McClelland J J 1995 *J. Opt. Soc. Am. B* **12** 1761
[21] Lee C J 2000 *Phys. Rev. A* **61** 063604
[22] Dalibard J and Cohen-Tannoudji C 1985 *J. Opt. Soc. Am. B* **2** 1707
[23] Meschede D and Metcalf H 2003 *J. Phys. D: Appl. Phys.* **36** R17
[24] Ramanlal P and Sander L M 1985 *Phys. Rev. Lett.* **54** 1828
[25] Dai G L, Koenders L, Pohlenz F, Dziomba T and Danzebrink H U 2005 *Meas. Sci. Technol.* **16** 1241